Appl. Phys. A 90, 457–463 (2008)
DOI: 10.1007/s00339-007-4303-3

Applied Physics A
Materials Science & Processing

TONG HONG WANG[1,2]
TE-HUA FANG[3]
YU-CHENG LIN[1,✉]

Finite-element analysis of the mechanical behavior of Au/Cu and Cu/Au multilayers on silicon substrate under nanoindentation

[1] Department of Engineering Science, National Cheng Kung University, Tainan 701, Taiwan, R.O.C.
[2] Thermal Laboratory, Advanced Semiconductor Engineering, Inc., Kaohsiung 811, Taiwan, R.O.C.
[3] Institute of Mechanical & Electromechanical Engineering, National Formosa University, Yunlin 632, Taiwan, R.O.C.

Received: 2 July 2007/Accepted: 21 September 2007
Published online: 30 October 2007 • © Springer-Verlag 2007

ABSTRACT Finite-element analysis of the nanoindentation into Au/Cu and Cu/Au multilayers was performed to deduce their mechanical characteristics from nanoindentation response. Different bilayer thicknesses, numbers, and sequences were studied using the load–displacement curve, hardness, indentation, and the residual surface profile as well as the von Mises equivalent stress. The characteristics of the multilayers were found to be dispersed between the Au and Cu. Nevertheless, if the indentation depth is smaller than the uppermost individual layer thickness of the multilayers, the intrinsic properties can be obtained. Using the von Mises equivalent stress as a failure criterion, the results showed that thinner multilayers would induce a greater potential of shear banding deformation.

PACS 61.43.Bn; 62.20.-x; 68.03.Hj; 68.05.Cf; 68.08.De

1 Introduction

Recently, multilayered thin films have created much interest due to their enhancing mechanical properties [1–5]. These multilayered thin films may be potential candidates for protecting, isolating, or other applications. Multilayered thin films prepared by the sputtering process can be a combination of metal, semiconductor, alloy, and other materials. For ease of fabrication, most multilayered studies only focus on bilayer or trilayer repeats. There are a number of low mutual solubility multilayered thin films like Cu/Ni, Ag/Ni, Au/Cu, and others, which produce sharp interfaces and do not form intermetallic compounds [1]. This is preferable for a basic study since intermetallic compounds may bring unknown mechanical properties.

Ruud et al. [1] measured the hardness and the elastic modulus of the Ag/Ni multilayered thin films, whose properties lie between those of homogeneous Ag and Ni thin films. They found a decrease in modulus at the smallest repeated length. Barshilia and Rajam [2] discovered that the hardness of the Cu/Ni multilayered thin films, with a total film thickness ranging between 68 and 90 Å, was enhanced by a factor of 2.5 times the rule of mixture. This enhancement in hardness is attributed to the arrest of the propagation of dislocations along the interfaces and a large number of interfaces in the multilayered coatings. Nevertheless, the hardness and effective Young's modulus of TiN/(Ti,Al)N multilayers [3] exhibited slightly higher values than monolithic TiN. This is thought to be due to either the higher covalence of the bonds in the (Ti,Al)N layer or a hardening effect related to the large number of interfaces which are present in the coating. Zhang et al. [4] demonstrated that the plastic deformation instability in Au/Cu multilayers becomes prevalent when the length scales of grains and the individual layer thickness of the multilayered composite approach the nanometer regime. However, the indentation depth of more than the total thickness of the multilayers must induce a large boundary effect from the substrate, bringing the intrinsic combined mechanical behaviors of Au/Cu multilayers in doubt.

Numerous compositions of layers have been studied for their mechanical behaviors. However, the study of the effects of different multilayer thicknesses, repeated numbers, and repeated sequences are insufficient, not to mention studies on the plastic-induced residual surface profile after indentation. This lack of research is mainly due to the high cost of both time and fabrication for such a large number of different combinations of multilayered thin films. To estimate the mechanical behavior of this particular structure, finite-element analysis (FEA) remains the preferred tool for the direct and economic way it provides to predict the mechanical response from the pre-set load. In the present study, we investigate nanoindentation on Au/Cu multilayers on silicon substrates of different bilayer thicknesses, numbers, and sequences by means of FEA. These low, mutually soluble multilayers were chosen because of the sharp interfaces, which can be analyzed numerically. The load–displacement curve, hardness, indentation, and residual surface profile, as well as von Mises equivalent stress are examined and compared in the present paper.

2 Finite-element modeling

The simulated sample in this study consisted of Au/Cu multilayers lying on a cylindrical silicon substrate. The diameter and the thickness of the silicon substrate are 7 μm and 10 μm, respectively. The Au/Cu multilayers have an identical individual layer thickness. A 1.5-μm-height

✉ Fax: +886-6-276-2329, E-mail: yuclin@mail.ncku.edu.tw

sharp diamond Berkovich indenter was simplified as a 70.3°-equivalent cone [5–7]. The multilayers, the bulk silicon, and the simplified Berkovich indenter are shown in Fig. 1a.

Due to the axial symmetry, only the portion from the center to the edge of the simulated sample, Fig. 1a, is modeled. The Berkovich indenter is simplified as a sharp indenter. This simplification may cause underestimation of the load–displacement curve for an actual tip in practice [8]. However, the curve pattern is proportional to the blunter tip. Thus, the present results might provide insight into the results corresponding to an indenter with a blunt tip. A two-dimensional finite-element model was built for the one-half cross-sectional simulated sample under the axisymmetric assumption, as shown in Fig. 1b. The model consists of 98 802 elements and 296 639 nodes. A quadratic quadrilateral element in which each element is defined by eight nodes was employed for the multilayers and the silicon substrate while a rigid line element was used for the indenter. The mesh is built up as a fine mesh near the contact region, gradually becoming coarser the farther away from the contact region to ensure its numerical efficiency and accuracy. Surface-to-surface contact elements are applied to the exposed surfaces which have the possibility of being touched. Symmetric boundary conditions were imposed on the symmetric plane of the simulated sample while vertical displacement was fixed on the substrate bottom. The modeling size and the mesh were tested and verified to be insensitive to the far-field boundary. The static analysis including large deflection was carried out using the commercial finite-element package ANSYS v.10.0.

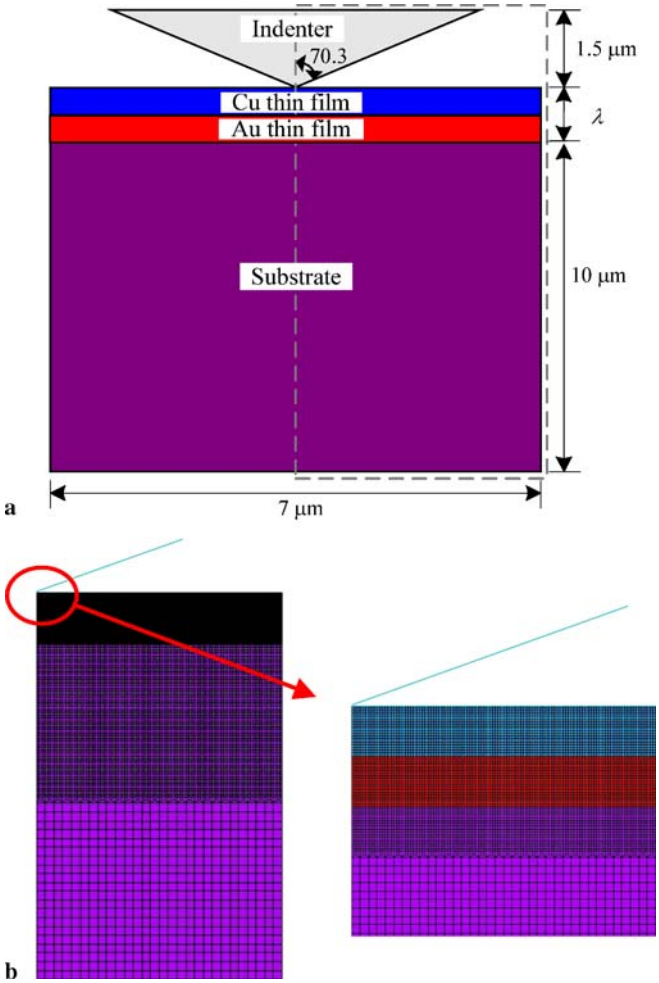

FIGURE 1 (**a**) Schematic diagram of the Cu/Au bilayer on silicon substrate (not to scale). The *dotted line* represents the modeling region, and (**b**) one-half of the finite-element meshes

The mechanical nature of a typical specimen can be described by a conventional stress–strain relationship that includes a strain-hardening exponent,

$$\sigma = E\varepsilon\,, \quad \text{for} \quad \varepsilon \le \sigma_y/E\,,$$
$$\sigma = K\varepsilon^m\,, \quad \text{for} \quad \varepsilon > \sigma_y/E\,, \tag{1}$$

where E is the Young's modulus, ε is the strain, σ_y is the yield stress, m is the strain-hardening exponent, and K is the strength coefficient and can be further defined as

$$K = \sigma_y(E/\sigma_y)^m\,, \tag{2}$$

to characterize the behavior at the onset of yield stress. This relationship can be converted to the multilinear kinematic hardening rule to be recognized by ANSYS. This option uses a von Mises yield criterion and is useful for large strain plasticity as the nanoindentation in this study. Material properties of the constitutive components [10–13] are listed in Table 1. In the table, E is the Young's modulus, σ_y the yield stress, m the strain-hardening exponent, and ν the Poisson's ratio. Generally speaking, the strain-hardening exponent of Si is supposed to be 0 and therefore Si behaves as an elastic-perfectly plastic [8, 9, 13]. The stress–strain behaviors of these constitutive components are schematically presented in Fig. 2. Comparatively, Si behaves as the hardest and the most brittle, Au behaves as the softest and the most flexible, and Cu lies somewhere in between. The coefficient of friction was previously proven to be minor [8, 13], especially for the indenters

Component	E (GPa)	σ_y (MPa)	m	ν
Au	82.7	207	0.02	0.42
Cu	110	52	0.54	0.343
Si	168	7000	0	0.28

TABLE 1 Material properties of the components

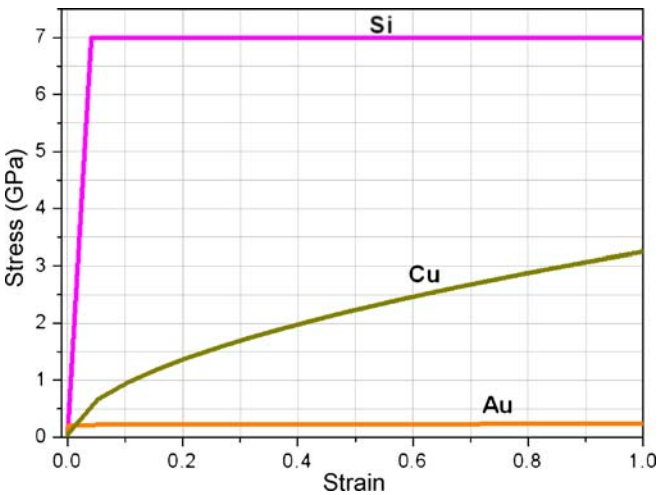

FIGURE 2 Stress–strain curves of Si, Cu, and Au

Test structure	λ (nm)	*n*
a	1000	1
b	500	2
c	250	5
d	100	10
e	50	20

TABLE 2 Test structures for different bilayer thicknesses and numbers of bilayers

having included angles greater than 60° [14]. Due to this, the coefficient of friction is assumed to be 0.1 for this study.

Table 2 lists the test structures examined in this study. First, three factors are investigated, i.e. bilayer thickness (λ), bilayer number (*n*), and the sequence. The λ of one *n* is composed of two equally thick Au and Cu layers. λ varies from 50, 100, 200, 500 to 1000 nm, and *n* varies from 1, 2, 5, 10 to 20, which means that all the test structures have an identical total multilayer thickness of 1000 nm. The third factor is the sequence. There are *n*(Cu/Au)/Si and *n*(Au/Cu)/Si stacking assemblies which represent *n* times the bilayers in the form of Cu/Au and Au/Cu with the bottom layers Au and Cu touching Si, respectively. The stacking of 1(Cu/Au)/Si is schematically shown in Fig. 1. The stacking sequence of 1(Au/Cu)/Si is reversed to that of 1(Cu/Au)/Si. For reference purposes, Au and Cu each with a total thickness of 1000 nm on Si are also included in this study.

The nanoindentation procedure is composed of loading and unloading. During loading, the indenter can be controlled by displacement or force and indents until the indenter reaches a pre-set maximum. During unloading, the indenter returns to its initial position. In order to prevent the substrate effect occurring from the Si in this study, an indentation depth of about one-tenth of the total thickness is recommended [15]. In this study we made an indent of 100 nm, one-tenth of the total thickness of the multilayer for characterizing the mechanical behavior of the multilayer as well as for the Au and Cu. Both loading and unloading will be separated by at least 50 substeps to ensure a stable convergence. The load–displacement curve is retrieved through the vertical reaction force and the displacement of the rigid indenter.

The hardness, H, is defined as the resistance to local deformation. It can be expressed as the indented load, P, divided by the contact area, A [16],

$$H = \frac{P}{A}, \tag{3}$$

where the contact area is a function of the contact depth, h_c, and can be determined according to the following form:

$$A = 24.5\, h_c^2. \tag{4}$$

The constant 24.5 is used for a perfect Berkovich indenter tip.

3 Results and discussion

3.1 *Load–displacement curve and hardness*

Figure 3 shows the load–displacement curves of the test structures for different bilayer thicknesses and numbers of bilayers. The load–displacement curves of Au and Cu are inset in each figure as reference curves. The curves of *n*(Au/Cu)/Si and *n*(Cu/Au)/Si are generally scattered between those of Au and Cu. Au shows a lower load along the indentation depth than Cu does owing to the higher stress–strain characterization of Cu compared to that of Au, as shown in Fig. 2. It is evident that for the two different sequences, the load–displacement curves of the thicker bilayers are closer to that of the bulk material when the uppermost layer is the same as the bulk material. This is reasonable since in this study the nanoindentation depth is 100 nm and can only penetrate the λ of 50 and 100 nm. In other words, the mutual effect will only be manifested at the individual layer thicknesses of 25 and 50 nm. Therefore, there is no doubt that the intrinsic behavior at the uppermost layer of the multilayers is similar to its bulk material when the indentation depth is smaller than its thickness. This is more obvious with a smaller indentation depth.

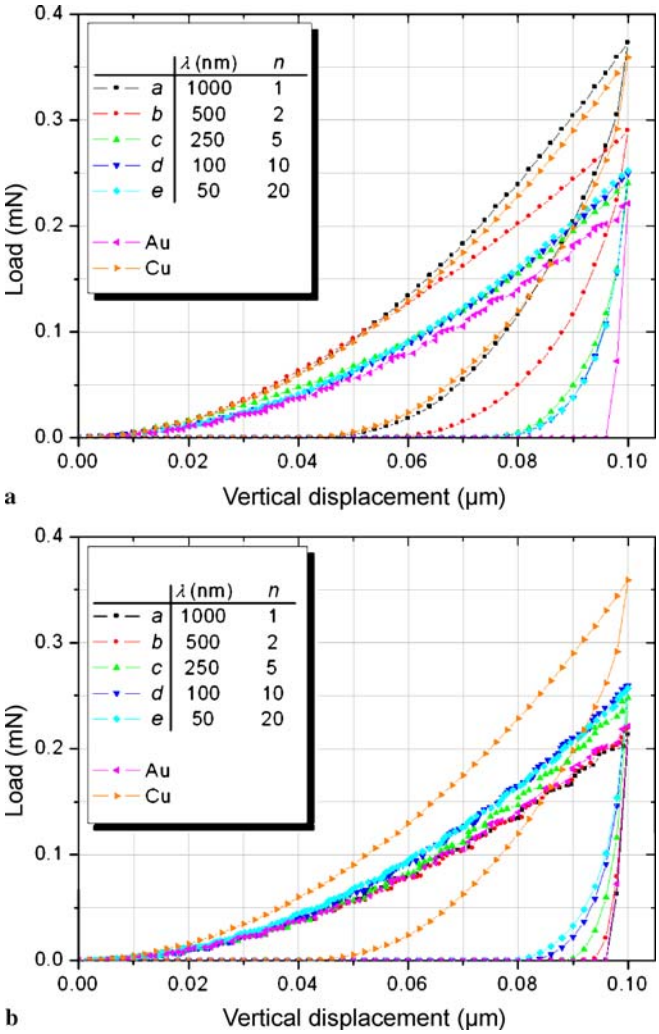

FIGURE 3 Load–displacement curve of (**a**) *n*(Cu/Au)/Si and (**b**) *n*(Au/Cu)/Si for different λ and *n*

Conventionally, hardness and Young's modulus are checked to verify the stability of the experiment and the analysis. In order to acquire a stable value we examined the hardness throughout the indentation depths during loading. Figure 4 shows the hardness–displacement curves of

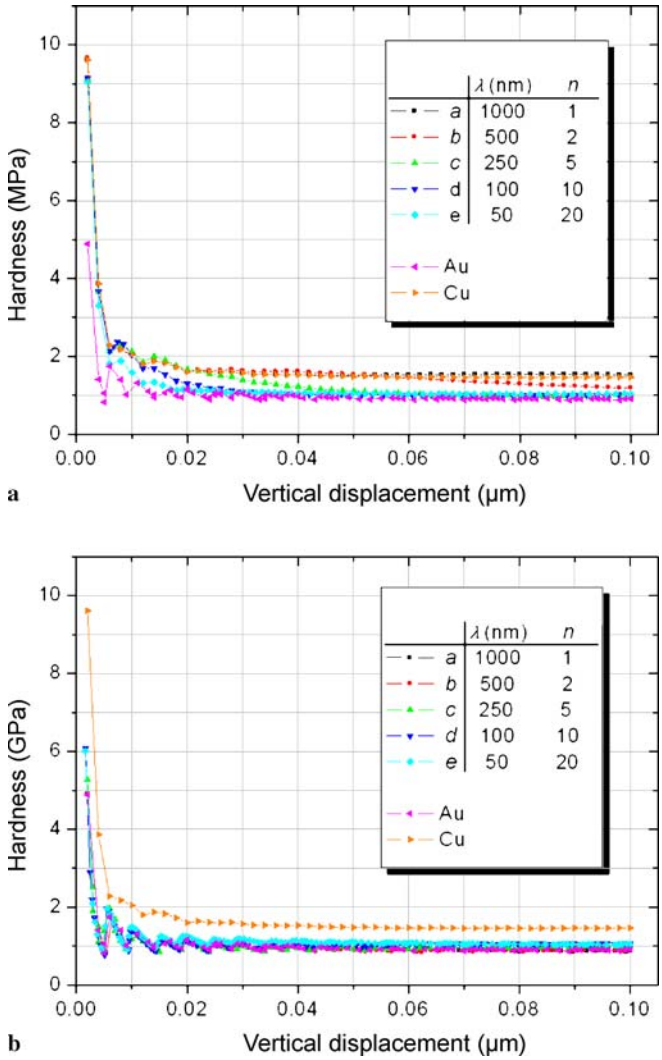

FIGURE 4 Hardness–displacement curves of (**a**) n(Cu/Au)/Si and (**b**) n(Au/Cu)/Si for different λ and n during loading

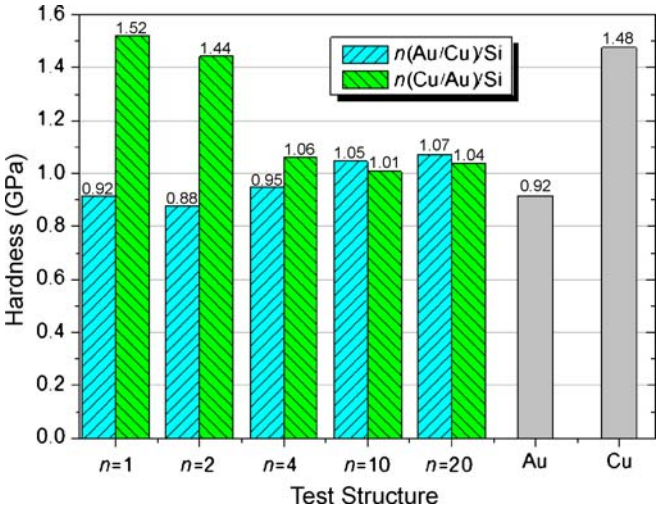

FIGURE 5 Average hardness of n(Cu/Au)/Si and n(Au/Cu)/Si for different test structures. The average hardness was calculated between the indentation depths of 40 and 80 nm

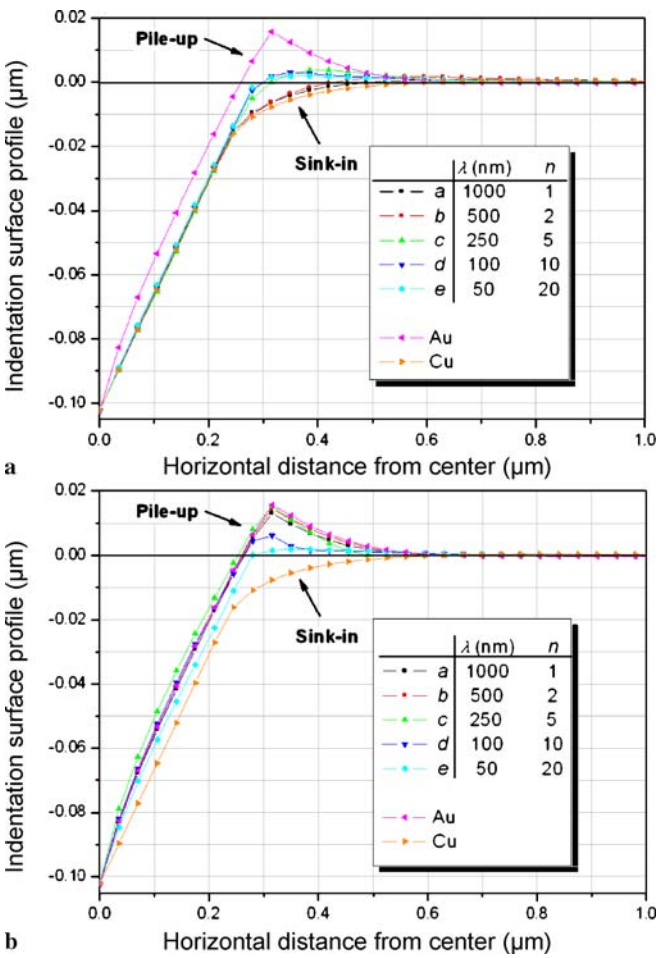

FIGURE 6 Indentation surface profiles of (**a**) n(Cu/Au)/Si and (**b**) n(Au/Cu)/Si for maximum nanoindentation depth

n(Cu/Au)/Si and n(Au/Cu)/Si for different λ and n. Among all the indentation depths, most hardnesses are found to stabilize in the range of 35 to 100 nm. Here, we averaged the hardness between the indentation depths of 40 and 80 nm as summarized in Fig. 5. Again, the data show that the hardnesses of n(Au/Cu)/Si and n(Cu/Au)/Si are scattered between the bulk Au and the bulk Cu. They resemble the aforementioned load–displacement curves in the sense that the behaviors depend on the thicknesses of the bilayers. The thicker the bilayer, the more alike the uppermost layer is to the same bulk material. On the contrary, the thinner the bilayer, the more the outcome will be like that of the combined properties.

3.2 *Indentation and residual surface profiles*

Figures 6 and 7 show the indentation and the residual surface profiles of n(Cu/Au)/Si and n(Au/Cu)/Si at maximum nanoindentation depth and after unloading, respectively. Again, the surface profiles of bulk Au and bulk Cu are inset in each figure as reference profiles. From these figures, pile-up of the Au and sink-in of the Cu is the highest and the deepest, respectively, among the test structures. These findings fully agree with the experimental findings from Fang et al. [17] and Fang and Chang [18]. It is evident from [5] that the pile-up is most pronounced for non- and nearly non-strain-

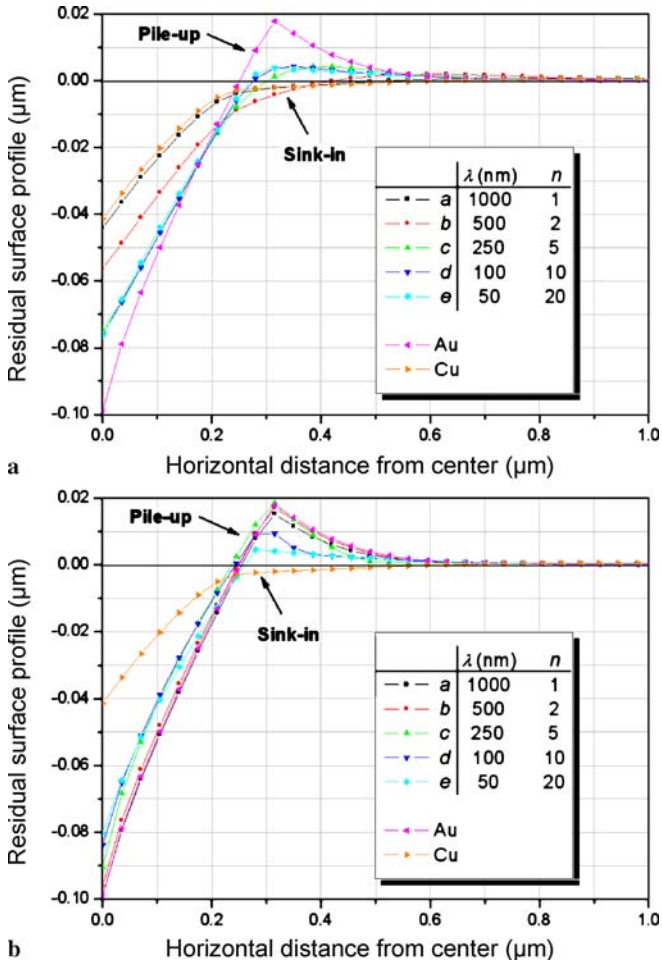

FIGURE 7 Residual surface profiles of (**a**) n(Cu/Au)/Si and (**b**) n(Au/Cu)/Si after unloading

hardening materials (Au's $m = 0.02$) while the sink-in is most pronounced for strain-hardening materials (Cu's $m = 0.54$).

Similar trends are quantifiable for the load–displacement curves where the surface profiles approach the uppermost layer when λ is thicker than the indentation depth. For instance, for the indentation surface profiles of n(Cu/Au)/Si, as shown in Fig. 6a, the profiles of the test structures *a* through *c* are close to that of the bulk Cu's profile, while those of n(Au/Cu)/Si, Fig. 6b, approach that of the bulk Au. For either n(Cu/Au)/Si or n(Au/Cu)/Si in which λ is less than the indentation depth, the test structures *d* and *e* show about average indentation surface profiles between bulk Au and bulk Cu. For the residual surface profiles, as plotted in Fig. 7, the aforementioned 'phenomenon' is more pronounced. There is a significant difference between n(Cu/Au)/Si and n(Au/Cu)/Si for certain λ of the test structures. Great elastic recoveries are observed for thicker λ of n(Cu/Au)/Si which are close to the intrinsic characteristics of bulk Cu. Comparatively speaking, there is less recovery for thicker λ of n(Au/Cu)/Si resembling that of bulk Au. As expected, the indentation and the residual surface profiles of the test structures *d* and *e* with smaller λ are scattered throughout due to the fact that the indentations pass through the interfaces.

3.3 *Shear banding potential*

Shear banding has been observed in submicrometer- to nanometer-scale materials, which is explained as the plastic deformation instability among the interfaces of multilayers [4]. Confinement between layers may lead to early failure and frequent fractures and may show as a wrinkle at the material's surface. However, the mechanisms of deformation are not yet well understood. Several stress indices are com-

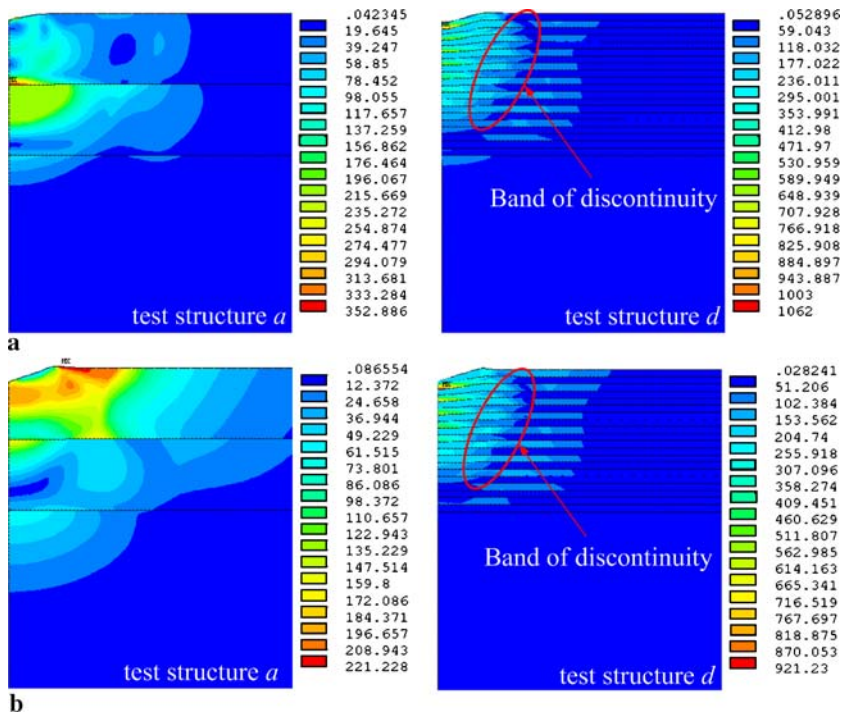

FIGURE 8 σ_{eqv} contours after unloading of (**a**) n(Cu/Au)/Si and (**b**) n(Au/Cu)/Si (unit: MPa)

monly used to investigate the possibility and the location of mechanical failures. Among them, the von Mises equivalent stress, σ_{eqv}, is defined by

$$\sigma_{eqv} = \sqrt{\frac{1}{2}\left[(\sigma_1-\sigma_2)^2+(\sigma_2-\sigma_3)^2+(\sigma_3-\sigma_1)^2\right]}, \quad (5)$$

where σ_1, σ_2, and σ_3 are the 1st, 2nd, and 3rd principal stresses, respectively. Yielding occurs when the equivalent stress exceeds the yield stress of the material, i.e. $\sigma_{eqv} > \sigma_y$.

Figure 8 shows the contour plots of σ_{eqv} on the multilayers after unloading of the test structures *a* and *d* with n(Cu/Au)/Si and n(Au/Cu)/Si, respectively. For n(Cu/Au)/Si with the test structures *a* and *d*, Fig. 8a, the maximum σ_{eqv} occurs around the bottom surface of the uppermost Cu layer right beneath the indenter at both test structures. This is acceptable because of the smaller yield stress of Cu compared to that of Au. Thus, Cu will show a larger plastic deformation at an earlier stage. Compared to all these, the test structure *e* with 50-nm-thick λ and 20*n* has the highest σ_{eqv}, while the test structure *a* with 1000-nm-thick λ and 1*n* is the lowest. This implies that a smaller λ induces a greater σ_{eqv} and causes earlier failure and possibly the initiation of shear banding deformation at the surface. Moreover, there is a significant band of σ_{eqv} discontinuity among the multilayers at the location we circled in Fig. 8. This discontinuity, however, could be realized in that the layers cannot easily move or slide in the in-plane direction owing to the limitation of different neighboring layers. In the meantime, in-plane plastic instability deformation is suppressed. Nevertheless, the slanted band tends the out-of-plane deformation, known as shear banding [19], has the potential of occurring. These trends are similar to the experimental observations of Zhang et al. [4] in that the shear banding becomes more prevalent with the decrease in individual layer thickness.

For n(Au/Cu)/Si with test structures *a* and *d*, Fig. 8b, the maximum σ_{eqv} occurs at the indented edge of the Au layer and around the bottom surface of the Cu layer at the second uppermost layer, respectively. Here, the test structure *a* is different from that of n(Cu/Au)/Si since, at such shallow (100-nm) indentation, the plastic deformation remains within the 500-nm-thick upper Au layer. For λ decreasing to 50-nm-thick individual layers of the test structure *d*, the softer second Cu layer beneath the uppermost Au layer suffers the maximum σ_{eqv}. Again, a significant σ_{eqv} discontinuity among multilayers occurs.

The corresponding maximum σ_{eqv} after unloading for different test structures are summarized in Fig. 9. By comparing the maximum σ_{eqv} on multilayers among the test structures, it is evident that the maximum σ_{eqv} of bulk Au and bulk Cu are the smallest compared to the others and the maximum σ_{eqv} of bulk Cu is smaller than that of bulk Au. Nevertheless, all of the maximum σ_{eqv} were greater than their yield stress, i.e. yielding developed. There is an obvious trend for the maximum σ_{eqv} to increase when λ decreases, which indicates that the thinner multilayers possess a greater potential for shear banding. Moreover, when comparing sequences with identical λ and *n*, the von Mises stresses of n(Au/Cu)/Si's are generally smaller than those of n(Cu/Au)/Si's. However, the difference

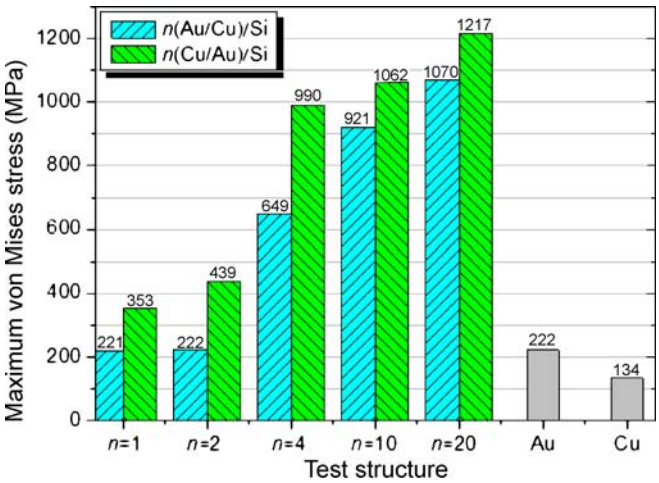

FIGURE 9 Maximum σ_{eqv} on multilayers after unloading for different test structures, bulk Au and bulk Cu

is quite small when λ is sufficiently thin, say 50-nm λ in the present study.

4 Conclusion

In this work, we investigated the mechanical characteristics of Au/Cu and Cu/Au multilayers. These multilayers had an identical total multilayer thickness of 1 μm with bilayers of different thicknesses, different numbers of bilayers, and different sequences on a silicon substrate by means of FEA. One-tenth of the total multilayer thickness, 100 nm, was chosen as the nanoindentation depth in order to prevent the substrate effect. Load–displacement curves, hardness, indentation, and residual surface profiles of Au and Cu multilayers were generally scattered between those of bulk Au and bulk Cu. For the two different bilayer sequences, the intrinsic behavior on the uppermost layer of the multilayers was similar to its bulk material for indentation depths that were smaller than its thickness. Furthermore, it was found that thinner multilayers will induce a greater von Mises stress and a significant band of stress discontinuity, indicating there is a greater potential for shear banding to take place.

ACKNOWLEDGEMENTS The authors would like to thank the National Science Council of Taiwan for the partial financial support under Grant Nos. NSC95-2221-E150-033 and NSC95-2221-E150-066.

REFERENCES

1 J.A. Ruud, T.R. Jervis, F. Spaepen, J. Appl. Phys. **75**, 4969 (1994)
2 H.C. Barshilia, K.S. Rajam, Surf. Coat. Technol. **155**, 195 (2002)
3 N.J.M. Carvalho, J.T.M. De Hosson, Acta Mater. **54**, 1857 (2006)
4 G.P. Zhang, Y. Liu, W. Wang, J. Tan, Appl. Phys. Lett. **88**, 013 105-1 (2006)
5 A.C. Fischer-Cripps, *Nanoindentation* (Springer, New York, 2002)
6 J.R. Barber, D.A. Bilings, Int. J. Mech. Sci. **32**, 991 (1990)
7 G.G. Bilodeau, J. Appl. Mech. **59**, 519 (1992)
8 T.H. Wang, T.H. Fang, Y.C. Lin, Mater. Sci. Eng. A **447**, 244 (2007)
9 T.H. Wang, T.H. Fang, Y.C. Lin, Appl. Phys. A **86**, 335 (2007)
10 A.W. Bowen, P.G. Partridge, J. Phys. D Appl. Phys. **7**, 969 (1973)
11 T. Li, Z.Y. Huang, Z. Suo, S.P. Lacour, S. Wagner, Appl. Phys. Lett. **85**, 3435 (2004)
12 J.H. Lau, Y.-H. Pao, *Solder Joint Reliability of BGA, CSP, Flip Chip and Fine Pitch SMT Assemblies* (McGraw-Hill, New York, 1997)

13 S.W. Youn, C.G. Kang, Mater. Sci. Eng. A **390**, 233 (2005)
14 J.L. Bucaille, S. Stauss, E. Felder, J. Michler, Acta Mater. **51**, 1663 (2003)
15 D. Beegan, M.T. Laugier, Surf. Coat. Technol. **199**, 32 (2005)
16 W.C. Oliver, G.M. Pharr, J. Mater. Res. **7**, 1564 (1992)
17 T.H. Fang, W.J. Chang, C.I. Weng, Mater. Sci. Eng. A **430**, 332 (2006)
18 T.H. Fang, W.J. Chang, Microelectron. Eng. **65**, 231 (2003)
19 L.J. Gibson, M.F. Ashby, *Cellular Solids: Structure and Properties* (Cambridge University Press, Cambridge, 1997)